Cover Article

A Cooperative Game-Theoretic Framework for Driver-Automation Interaction Control with Online Identification of Drive Steering Characteristics

Yue Liu and Simon Hu

***Abstract*—This paper proposes a cooperative game-theoretic framework for driver-automation interaction control. It features personalized assistance through online identification of driver steering characteristics. A two-point preview-based distributed model predictive control (MPC) strategy is developed to model the interactive behaviour between the human driver and the active front steering (AFS) system of a passenger car. The proposed strategy leverages cooperative game theory, formulating a joint optimisation of the steering actions of both the driver and the AFS based on Pareto equilibrium. To account for inter-driver variability in steering behaviour and deliver tailored assistance, a recursive least squares (RLS) algorithm with exponential forgetting is applied to identify driver steering characteristics online. The estimated driver steering characteristics are then used to compute the AFS steering angle that supports the driver's steering actions. Two numerical studies are carried out. The first study demonstrates the effectiveness of the Pareto-equilibrium steering strategies, incorporating the two-point-preview setup in achieving satisfactory vehicle path-tracking performance. The second study validates the proposed online identification scheme under different driver-imposed path-tracking penalties as well as different weight allocations between the driver and the AFS controller.**

***Index Terms*—Driver-automation interaction, modelling, cooperative game, online identification**

I. Introduction

INAPPROPRIATE driving behaviors, such as driving under the influence, fatigue, poor driving skills, and operational errors, remain amongst the primary causes of traffic accidents [1–3]. Meanwhile, the growing number of vehicles has led to significant rise in energy consumption and severe traffic congestion, resulting in huge economic losses. Intelligent vehicles have the potential to address these issues, with fully autonomous vehicles representing the ultimate vision. However, vehicles equipped with the state-of-the-art automated driving technologies continue to exhibit technical limitations when tested in complex real-world conditions, raising ongoing concerns regarding their social, ethical, and legal implications. Therefore, it remains necessary for human drivers to retain control of vehicles.

Nowadays, advanced driver assistance systems (ADASs), featuring accurate perception and precise control capabilities are increasingly capable of supporting drivers in performing various driving tasks while reducing cognitive and physical workload. Moreover, the integration of existing controlled monitoring systems can enhance the quality of decisions [4]. However, the intervention of such systems sometimes can interfere with driver intentions, potentially compromising vehicle safety and stability. For instance, a scenario involving a vehicle equipped with an ADAS is able to detect, evaluate, and autonomously conduct evasive steering manoeuvres to avoid potential collisions. If a pedestrian suddenly enters the roadway, the automated system may initiate an evasive steering manoeuvre based on a predefined decision-making strategy. In contrast, the human driver might prefer to decelerate while maintaining a straight trajectory, anticipating that the pedestrian will clear the road promptly. This divergence in decision-making introduces a conflict between the driver's intent and the system's response. Addressing this driver-automation interaction in conflicting scenarios remains a key challenge in the development of next-generation ADAS.

To address the potential conflict between human driver and vehicle automation, Scholtens et al. [5] proposed a so-called "four-design-choice-architecture" for driver-automotive shared control, in which feed-forward torque assistance along with a reference trajectory aligned with the driver's intent were employed to reduce conflict. Zwaan et al. [6] introduced an adaptive authority allocation strategy between feedback and feedforward steering torques, wherein the relative contributions of each component were dynamically adjusted based on driving conditions. Nguyen et al. [7] proposed a shared control strategy that evaluated the driver's real-time behavioural competence and accordingly computed the optimal assistance torque to align with the driver's capability, thereby reducing the conflict between driver and assistance systems. Following this work, Oudainia et al. [8] employed a

Manuscript received: 3 June 2025; revised: 10 July 2025; accepted: 16 July 2025. *(Corresponding author: Simon Hu.)*

Citation: Y. Liu and S. Hu, A cooperative game-theoretic framework for driver-automation interaction control with online identification of drive steering characteristics, *Int. J. Intell. Control Syst.*, 2025, 30(3), 193–206.

Yue Liu and Simon Hu are with Zhejiang University-University of Illinois at Urbana-Champaign Institute, Zhejiang University, Haining 314400, China (e-mail: 0623320@zju.edu.cn; simonhu@zju.edu.cn).

Simon Hu is also with Department of Civil and Environmental Engineering, Imperial College, London SW7 2BU, UK.

Digital Object Identifier 10.62678/IJICS202509.10164

control strategy aiming at alleviating driver-automation conflicts by simultaneously considering the driver's real-time driving performance and external risk factors, such as the potential risk of collision with pedestrians. Chen et al. [9] developed a shared control method based on driver state prediction, allowing assistant torque to align with the driver's steering behaviour. Han et al. [10] proposed an approach to address human-machine interaction based on the concept of variable-impedance, in which reinforcement learning was employed to adaptively adjust the interaction dynamics. Ding et al. [11] developed a correlation-based control method that statistically analysed the relationship between driver and assistance torques to enable adaptive authority distribution. Lu et al. [12] proposed a fuzzy control strategy that accounted for driver behaviour uncertainty and system constraints, utilising pre-collected steering data to quantify driver performance and adjust the assistance torque accordingly.

The aforementioned studies have demonstrated the feasibility of alleviating conflicts between human drivers and vehicle automation. However, the absence of a theoretical framework capable of characterising the underlying mechanism of driver-automation interaction limits the theoretical development and poses uncertainty in the generalisation of these methods. To address this challenge, Na and Cole [13–15] proposed a set of game-theoretic modelling paradigms, pioneering the integration of dynamic game theory and model predictive control (MPC), to characterize the fundamental principles governing the interaction between human driver and vehicle automation in the context of active front steering (AFS) intervention. Although their works primarily focus on modelling the interactive behaviour between human driver and AFS, without proposing corresponding shared control strategies for vehicle automation, their game-theoretic insights lay a solid foundation for subsequent developments in shared control methodologies. Based on the framework proposed by Refs. [13–15], Ji et al. [16] developed a control strategy grounded on stochastic non-cooperative game theory, explicitly accounting for uncertainties in driver behaviour. Li et al. [17] proposed a shared control approach based on a non-zero-sum dynamic game, in which an adaptive dynamic programming algorithm was employed to compute the Nash equilibrium between driver and vehicle automation. Yang et al. [18] developed a driver assistance control algorithm featuring adaptively adjusting preview time and control gains to emulate human driving behaviour. Recently, Liu et al. [19] proposed a master-slave-based strategy for dynamic driving authority adjustment, formulating the implicit competition between driver and automation as a hierarchical game, and employing a hybrid method for prior authority allocation. Liang et al. [20] introduced a driver-automation shared steering system considering the CAN-delay, to reduce the communication load and improve the usage of network resources. In addition, studies on driver-automotive shared control can be extended by referring to state-of-the-art research on parallel control and/or cooperative control of subsystems. For instance, Jiao et al. [21] proposed an innovative consensus control strategy, which belonged to a classic cooperative control approach, for uncertain multi-agent systems. Lu et al. [22] developed an event-based control method for cooperative adaptive cruise control systems using parallel control, to optimise the control and communication of connected vehicles.

Despite the extensive research on the practical implementation and theoretical development of driver-automation shared control, very limited attention has been paid to the behavioral diversity among drivers in the context of shared control. In the real-world scenarios, drivers can exhibit distinct steering characteristics, leading to substantial variations in the associated characteristic parameters in control algorithms. This variability poses a fundamental challenge: the need to design shared control strategies that are both broadly applicable across diverse driver populations and capable of providing personalized assistance. Although Fang et al. [23] proposed a driver-automation shared control framework considering driver's time-varying characteristics, they mainly focus on the driver's intention and ability, instead of the present characteristics that represent the driver's penalization of vehicle path-tracking errors. These characteristics are strongly affected by the driver's physical and psychological states.

Towards this challenge, a driver-automation shared control strategy is developed and investigated in this paper, aiming to mitigate driver-automation conflict while delivering assistance tailored to individual drivers according to the driver's present driving characteristics. The core contributions of this work are as follows:

(1) To overcome the limitation of conventional driver models in capturing the influence of vehicle automation on driver steering behaviour, a cooperative game-theoretic framework is proposed to model the interaction between driver and automation. The model is derived based on a two-point preview setup to facilitate the online identification of driver steering characteristics.

(2) To account for the variation of driver steering control behaviour, an online identification approach based on recursive least squares (RLS), which augmented by the exponential forgetting and resetting algorithm (EFRA), is developed to estimate the driver steering characteristics in the real time.

The remainder of this paper is organized as follows. Section II describes the vehicle dynamics and path prediction models of driver and AFS system. Section III formulates the analytical derivation of the driver and AFS system cooperative Pareto steering strategies. Online identification method of driver steering characteristics is then introduced in detail in Section IV. Section V states numerical studies to validate the proposed driver and AFS cooperative game-theoretic steering strategy. Section VI draws conclusions and suggests the future work.

II. Vehicle Dynamics and Distributed Model Predictive Control

This section describes the dynamics model characterizing the driver-vehicle closed-loop system. In the context of driver steering behaviour modelling, MPC has been widely recognized as an effective approach, as it aligns with the widely adopted "internal model" hypothesis in neuroscience [24]. The applicability of MPC-based models capturing driver steering behaviour has been extensively validated through experimental studies, e.g., Refs. [15, 25, 26]. Building on this foundation, and considering that the driver and automation possess independent perception, decision-making and control capabilities, a distributed model predictive control (DMPC) approach is proposed to model their steering control behaviour independently. This formulation allows the extension of MPC to multi-agent applications, thereby preserving the fundamental structure required for modelling driver-automation shared control.

The vehicle automation considered in the context of this work is the AFS system [27], which has been widely recognized as a practical platform for implementing driver-automation shared control.

A. Vehicle Dynamics

The front wheel steering angle of the vehicle can be determined as the sum of steering angle applied by the driver and that applied by the AFS system. Accordingly, the dynamics of the vehicle can be described using the following state-space representation

$$\dot{x}_{\mathrm{C}}(t) = A_{\mathrm{C}}x_{\mathrm{C}}(t) + B_{\mathrm{C}1}\delta_1(t) + B_{\mathrm{C}2}\delta_2(t) \tag{1}$$

where

$$x_{\mathrm{C}}(t) = [v(t) \quad \omega(t) \quad y(t) \quad \psi(t)]^{\mathrm{T}} \tag{2}$$

$$A_{\mathrm{C}} = \begin{bmatrix} \dfrac{-(C_{\mathrm{f}}+C_{\mathrm{r}})}{Um} & \dfrac{-(aC_{\mathrm{f}}-bC_{\mathrm{r}})}{Um} - U & 0 & 0 \\ \dfrac{-(aC_{\mathrm{f}}-bC_{\mathrm{r}})}{UI} & \dfrac{-(a^2C_{\mathrm{f}}+b^2C_{\mathrm{r}})}{UI} & 0 & 0 \\ 1 & 0 & 0 & U \\ 0 & 1 & 0 & 0 \end{bmatrix} \tag{3}$$

$$B_{\mathrm{C}1} = \begin{bmatrix} \dfrac{C_{\mathrm{f}}}{mG} & \dfrac{aC_{\mathrm{f}}}{IG} & 0 & 0 \end{bmatrix}^{\mathrm{T}} \tag{4}$$

$$B_{\mathrm{C}2} = \begin{bmatrix} \dfrac{C_{\mathrm{f}}}{mG} & \dfrac{aC_{\mathrm{f}}}{IG} & 0 & 0 \end{bmatrix}^{\mathrm{T}} \tag{5}$$

where $v(t)$ is the vehicle lateral speed, $\omega(t)$ is the yaw rate, $y(t)$ is the lateral displacement, and $\psi(t)$ is the yaw angle. δ_1 is the steering wheel angle applied by the human driver and δ_2 is the steering angle generated by the AFS system. U denotes the longitudinal velocity of the vehicle, m denotes the vehicle mass, I denotes the total yaw moment of inertia, and G denotes the gear ratio of the steering system. a and b denote the distances from the vehicle's centre of gravity to the front and rear axles respectively. C_{f} and C_{r} denote the equivalent cornering stiffness of the front and rear axles respectively. By discretizing the continuous system described by Eq. (1), the following discrete-time representation can be obtained

$$x_{\mathrm{D}}(k+1) = A_{\mathrm{D}}x_{\mathrm{D}}(k) + B_{\mathrm{D}1}\delta_1(k) + B_{\mathrm{D}2}\delta_2(k) \tag{6}$$

where $x_{\mathrm{D}}(k) = [v(k) \ \omega(k) \ y(k) \ \psi(k)]^{\mathrm{T}}$, denoting the discrete state vector. To facilitate the control of vehicle directional dynamics, an additional state variable $y_{int}(k)$, representing the time integral of the lateral displacement $y(t)$ is introduced, where $y_{int}(k+1) = y_{int}(k) + y(k)$. Therefore, the discrete system described by Eq. (6) can be augmented to

$$\begin{aligned} x(k+1) &= Ax(k) + B_1\delta_1(k) + B_2\delta_2(k), \\ z(k) &= Cx(k) \end{aligned} \tag{7}$$

where $x(k) = [v(k) \ \omega(k) \ y(k) \ \psi(k) \ y_{int}(k)]^{\mathrm{T}}$ is state vector of the augmented system. $z(k) = [y(k) \ y_{int}(k)]^{\mathrm{T}}$ denotes the system output. A, B_1, B_2, and C are system matrix, input matrices, and output matrix, respectively.

It should be noted that in the real-world driving conditions, vehicle dynamics may exhibit nonlinear and time-varying characteristics, because of the operational factors such as the variation of tyre cornering stiffness with tyre sideslip angle. In this study, to reduce the complexity of the human-vehicle closed-loop dynamics and thus focus on the behavioral interaction between the driver and automation, the linear time-invariant discrete-time system described by Eq. (7) is used. In the subsequent numerical analysis, particular attention is paid to the design of testing scenarios, in which moderate-intensity lane-change is considered to ensure that the vehicle dynamics remain within the linear operating range, thus satisfying the linear time-invariant assumptions underlying the discrete-time system in Eq. (7).

B. Path Prediction of Driver and AFS

The vehicle future path predicted by the driver can be derived by iterating Eq. (7). This is started by determining the system output at time step $k+2$ as described below.

$$\begin{aligned} z(k+2) &= Cx(k+2) = \\ &CAx(k+1) + CB_1\delta_1(k+1) + CB_2\delta_2(k+1) = \\ &CA^2x(k) + CAB_1\delta_1(k) + CAB_2\delta_2(k) + \\ &CB_1\delta_1(k+1) + CB_2\delta_2(k+1) \end{aligned} \tag{8}$$

By continuing the iteration, system outputs at $z(k+3)$ up to $z(k+N_1)$, where N_1 represents preview horizon of the human driver, can be obtained. Therefore, the driver's predicted vehicle path at time step k can be formulated as

$$Z_1(k) = \Psi_1 x(k) + \Theta_1 U_1(k) + \Omega_1 U_2(k) \tag{9}$$

where

$$Z_1(k) = [z(k) \quad z(k+1) \quad z(k+2) \ \cdots \ z(k+N_1)]^{\mathrm{T}} \tag{10}$$

$$U_1(k) = [\delta_1(k) \ \delta_1(k+1) \ \delta_1(k+2) \ \cdots \ \delta_1(k+N_1-1)]^{\mathrm{T}} \tag{11}$$

$$U_2(k) = [\delta_2(k) \ \delta_2(k+1) \ \delta_2(k+2) \ \cdots \ \delta_2(k+N_1-1)]^{\mathrm{T}} \tag{12}$$

$$\Psi_1 = \begin{bmatrix} C & CA & CA^2 & \cdots & CA^{N_1} \end{bmatrix} \tag{13}$$

$$\Theta_1 = \begin{bmatrix} 0 & 0 & 0 & \cdots & 0 \\ 0 & CB_1 & 0 & \cdots & 0 \\ 0 & CAB_1 & CB_1 & \cdots & 0 \\ \vdots & \vdots & \vdots & \ddots & \vdots \\ 0 & CA^{N_1-1}B_1 & CA^{N_1-2}B_1 & \cdots & CB_1 \end{bmatrix} \tag{14}$$

$$\Omega_1 = \begin{bmatrix} 0 & 0 & 0 & \cdots & 0 \\ 0 & CB_2 & 0 & \cdots & 0 \\ 0 & CAB_2 & CB_2 & \cdots & 0 \\ \vdots & \vdots & \vdots & \ddots & \vdots \\ 0 & CA^{N_1-1}B_2 & CA^{N_1-2}B_2 & \cdots & CB_2 \end{bmatrix} \tag{15}$$

It is worth noting that vector $U_1(k)$ contains a number of N_1+1 elements, with $\delta_1(k+j)$, $j = 0, 1, \ldots, N_1 - 1$ representing the future steering angle to be applied by the driver. For this study, the driver's steering angle is kept unchanged within the preview horizon, according to the analysis provided by Na and Cole [15]. Such a treatment also complies with the observation provided by Ungoren and Peng [25]. As a result, Eq. (9) reduces to

$$Z_1(k) = \tilde{\Psi}_1 x(k) + \tilde{\Theta}_1 \delta_1(k) + \tilde{\Omega}_1 \delta_2(k) \tag{16}$$

where

$$Z_1(k) = \begin{bmatrix} z(k) \\ z(k+1) \\ z(k+2) \\ \vdots \\ z(k+N_1) \end{bmatrix} \tag{17}$$

$$\tilde{\Psi}_1 = \begin{bmatrix} C \\ CA \\ CA^2 \\ \vdots \\ CA^{N_1} \end{bmatrix} \tag{18}$$

$$\tilde{\Theta}_1 = \begin{bmatrix} 0 \\ CB_1 \\ \sum_{i=0}^{1} CA^i B_1 \\ \vdots \\ \sum_{i=0}^{N_1-1} CA^i B_1 \end{bmatrix} \tag{19}$$

$$\tilde{\Omega}_1 = \begin{bmatrix} 0 \\ CB_2 \\ \sum_{i=0}^{1} CA^i B_2 \\ \vdots \\ \sum_{i=0}^{N_1-1} CA^i B_2 \end{bmatrix} \tag{20}$$

$$\tilde{\Psi} = \begin{bmatrix} C & CA & CA^2 & \cdots & CA^{N_1} \end{bmatrix}^{\mathrm{T}} \tag{21}$$

By following the same derivation, the path prediction for the AFS system can be obtained as

$$Z_2(k) = \tilde{\Psi}_2 x(k) + \tilde{\Theta}_2 \delta_1(k) + \tilde{\Omega}_2 \delta_2(k) \tag{22}$$

where

$$Z_2(k) = \begin{bmatrix} z(k) \\ z(k+1) \\ z(k+2) \\ \vdots \\ z(k+N_2) \end{bmatrix} \tag{23}$$

$$\tilde{\Psi}_2 = \begin{bmatrix} C \\ CA \\ CA^2 \\ \vdots \\ CA^{N_2} \end{bmatrix} \tag{24}$$

$$\tilde{\Theta}_2 = \begin{bmatrix} 0 \\ CB_1 \\ \sum_{i=0}^{1} CA^i B_1 \\ \vdots \\ \sum_{i=0}^{N_2-1} CA^i B_1 \end{bmatrix} \tag{25}$$

$$\tilde{\Omega}_2 = \begin{bmatrix} 0 \\ CB_2 \\ \sum_{i=0}^{1} CA^i B_2 \\ \vdots \\ \sum_{i=0}^{N_2-1} CA^i B_2 \end{bmatrix} \tag{26}$$

where N_2 represents the preview horizon of AFS system.

To facilitate the development of the cooperative driver-automation shared control framework, we assume that the driver and AFS have the same preview horizon, i.e., $N_1 = N_2 = N$. It is worth noting that this assumption holds in real-world vehicle applications, as the automation systems are typically configured to exhibit preview behaviour comparable to that of human drivers. For generality, N_1 and N_2 are still used subsequently.

In this work, the preview times for both the driver and AFS system are 2 s. This suggests when the discrete time interval T is set as 0.01 s, the preview horizons of the driver and AFS are both of 200 steps. Therefore, as indicated by Eqs. (6) and (7), both $Z_1(k)$ and $Z_2(k)$ are column vectors of 402 rows and the dimensions of $\tilde{\Psi}_1$ and $\tilde{\Psi}_2$ are both 402 × 5. This would place a computational burden on determining the optimal steering angles of the driver, and making it unsuitable for the online identification of driver behaviour.

To reduce the dimensions of the vectors and matrices involved in Eqs. (16) and (22) and facilitate the online identification of the driver steering characteristics (to be discussed later), we adopt the "two-point preview" setup for both the driver and AFS system. This involves selecting only the middle point and the end point within the preview horizon N. Consequently, the driver's path prediction grounded on the two-point preview can be formulated as

$$\hat{Z}_1(k) = \hat{\Psi}_1 x(k) + \hat{\Theta}_1 \delta_1(k) + \hat{\Omega}_1 \delta_2(k) \tag{27}$$

where

$$\hat{Z}_1(k) = \begin{bmatrix} z(k) \\ z(k+N_1/2) \\ z(k+N_1) \end{bmatrix} \tag{28}$$

$$\hat{\Psi}_1 = \begin{bmatrix} C \\ CA^{N_1/2} \\ CA^{N_1} \end{bmatrix} \tag{29}$$

$$\hat{\Theta}_1 = \begin{bmatrix} 0 \\ \sum_{i=0}^{N_1/2-1} CA^i B_1 \\ \sum_{i=0}^{N_1-1} CA^i B_1 \end{bmatrix} \tag{30}$$

$$\hat{\Omega}_1 = \begin{bmatrix} 0 \\ \sum_{i=0}^{N_1/2-1} CA^i B_1 \\ \sum_{i=0}^{N_1-1} CA^i B_1 \end{bmatrix} \tag{31}$$

Similarly, the AFS system's path prediction can be described as

$$\hat{Z}_2(k) = \hat{\Psi}_2 x(k) + \hat{\Theta}_2 \delta_1(k) + \hat{\Omega}_2 \delta_2(k) \tag{32}$$

where

$$\hat{Z}_2(k) = \begin{bmatrix} z(k) \\ z(k+N_2/2) \\ z(k+N_2) \end{bmatrix} \tag{33}$$

$$\hat{\Psi}_2 = \begin{bmatrix} C \\ CA^{N_2/2} \\ CA^{N_2} \end{bmatrix} \tag{34}$$

$$\hat{\Theta}_2 = \begin{bmatrix} 0 \\ \sum_{i=0}^{N_2/2-1} CA^i B_1 \\ \sum_{i=0}^{N_2-1} CA^i B_1 \end{bmatrix} \tag{35}$$

$$\hat{\Omega}_2 = \begin{bmatrix} 0 \\ \sum_{i=0}^{N_2/2-1} CA^i B_1 \\ \sum_{i=0}^{N_2-1} CA^i B_1 \end{bmatrix} \tag{36}$$

Combining Eqs. (27) and (32) gives the formulation of the global path prediction

$$Z(k) = \bar{\Psi} x(k) + \bar{\Theta} \delta_1(k) + \bar{\Omega} \delta_2(k) \tag{37}$$

where

$$Z(k) = \begin{bmatrix} \hat{Z}_1(k) \\ \hat{Z}_2(k) \end{bmatrix} \tag{38}$$

$$\bar{\Psi} = \begin{bmatrix} \hat{\Psi}_1 \\ \hat{\Psi}_2 \end{bmatrix} \tag{39}$$

$$\bar{\Theta} = \begin{bmatrix} \hat{\Theta}_1 \\ \hat{\Theta}_2 \end{bmatrix} \tag{40}$$

$$\bar{\Omega} = \begin{bmatrix} \hat{\Omega}_1 \\ \hat{\Omega}_2 \end{bmatrix} \tag{41}$$

III. Cooperative Game-Theoretic Steering Strategy for Driver-AFS Shared Control

This section introduces the cooperative game-theoretic framework of driver-AFS interaction and the principle of the Pareto-equilibrium strategies. Based on this, derivation of the steering strategies for the driver and the active front steering system are detailed.

A. Cooperative Game-Theoretic Driver-AFS Interaction

Fig. 1 illustrates the cooperative game-theoretic framework underpinning the interaction between the driver and AFS system. As shown in Fig. 1, the driver and AFS system are capable of determining their steering control strategies independently. Specifically, at time step k, drivers can account for the vehicle state $x(k)$, their own target path $R_1(k)$, the AFS controller's target path $R_2(k)$, and the AFS controller's steering action $\delta_2(k)$, when formulating the driver's steering strategy. Similarly, the AFS system determines its control strategy by taking the vehicle state $x(k)$, its own target path $R_2(k)$, the driver's target trajectory $R_1(k)$, and steering action $\delta_1(k)$ into account. As shown in Fig. 1, the driver's steering action $\delta_1(k)$ and the AFS system's steering action $\delta_2(k)$ are blended within the planetary gear system of active front steering.

The decision-making processes of the driver and AFS controller described above can be represented using the following two functions following the analysis of Na and Cole [14].

$$\delta_1(k) = f_1(x(k),\ R_1(k),\ R_2(k),\ \delta_2(k)) \tag{42}$$

$$\delta_2(k) = f_2(x(k),\ R_2(k),\ R_1(k),\ \delta_1(k)) \tag{43}$$

where $f_1(\cdot)$ and $f_2(\cdot)$ represent the mapping rules for the driver and AFS system, respectively.

It is worth noting that the concept expressed in Eq. (1) is practically justifiable. For example, after the vehicle automation system plans its own target path at time step k, this information can be communicated to the driver via an on-board display. In addition, the system's planned steering actions can be conveyed to the driver through visual cues or haptic feedback. These feedback mechanisms enable the driver to be aware of the vehicle automation's intention. Consequently, drivers can take this into consideration and apply Eq. (1) to determine their own steering control strategy.

Likewise, the principle described by Eq. (6) is operationally applicable. In this context, the driver's steering action $\delta_1(k)$ can be measured using a steering wheel angle sensor, which is commonly installed in road vehicles equipped with dynamic stability control systems. The driver's intended path $R_1(k)$ can

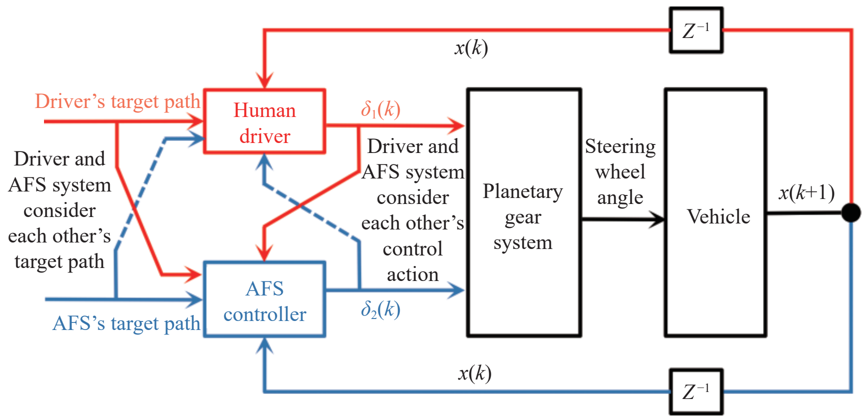

Fig. 1 Cooperative game-theoretic framework of driver-AFS interaction.

be estimated through various driver intention recognition algorithms, such as those discussed in Ref. [28].

B. Pareto Strategy of Driver and AFS

Within the theoretical framework of game theory, the concept of "equilibrium" refers to a state in which no game player has an incentive to unilaterally alter its strategy, as such a change would yield no additional benefit [13]. In the context of cooperative games, this state is referred to a Pareto equilibrium, whereas in non-cooperative games, it corresponds to the well-known Nash equilibrium. The set of strategies adopted by all players at a Pareto equilibrium is thus termed their Pareto strategies. Applying this concept to the cooperative interaction between the driver and AFS system described above, the Pareto strategies of the driver and AFS can be expressed as

$$\delta_1{}^*(k) = f_1{}^*(x(k),\, R_1(k),\, R_2(k),\, \delta_2(k)) \tag{44}$$

$$\delta_2{}^*(k) = f_2{}^*(x(k),\, R_2(k),\, R_1(k),\, \delta_1(k)) \tag{45}$$

where $\delta_1{}^*(k)$ and $\delta_2{}^*(k)$ respectively represent the steering actions of the driver and the AFS at a Pareto equilibrium and $f_1{}^*(\cdot)$ and $f_2{}^*(\cdot)$ are respectively the mapping rules corresponding to the Pareto equilibrium.

To derive the analytical expressions of the driver's and AFS's Pareto steering control strategies, it is necessary to construct the two controllers' respective objective functions, which begins with defining their target paths.

For the driver, the target path $R_1(k)$ can be represented as a vector comprising planned trajectory information at three reference points, corresponding to the current time step k, future time steps $k+N_1/2$ and $k+N_1$, respectively. The latter two reference points are consistent with the two-point preview setup introduced earlier. Hence, the driver's target path $R_1(k)$ can be expressed as

$$R_1(k) = \begin{bmatrix} r_1(k) \\ r_1\left(k+\dfrac{N_1}{2}\right) \\ r_1(k+N_1) \end{bmatrix}, \qquad r_1(k+j) = \begin{bmatrix} r_1^y(k+j) \\ r_1^{yint}(k+j) \end{bmatrix},\ j = 0,\ \frac{N_1}{2},\ N_1 \tag{46}$$

In Eq. (46), each $r_1(k+j)$ incorporates two aspects trajectory information: reference vehicle lateral displacement r_1^y and its integral r_1^{yint}.

Similarly, the AFS controller's target path $R_2(k)$ can be expressed as

$$R_2(k) = \begin{bmatrix} r_2(k) \\ r_2(k+\dfrac{N_1}{2}) \\ r_2(k+N_1) \end{bmatrix}, \qquad r_2(k+j) = \begin{bmatrix} r_2^y(k+j) \\ r_2^{yint}(k+j) \end{bmatrix},\ j = 0,\ \frac{N_2}{2},\ N_2 \tag{47}$$

At time step k, drivers' objective can be described as minimizing their path-tracking error $E_1(k) = R_1(k) - \hat{Z}_1(k)$, where $\hat{Z}_1(k)$ is the predicted path of the driver, as described by Eq. (27). Similarly, the AFS system aims to minimize its own path-tracking error $E_2(k) = R_2(k) - \hat{Z}_2(k)$, where $\hat{Z}_2(k)$ is the AFS system's predicted path determined by Eq. (32).

As explained previously, in the cooperative-game framework, each player considers not only their own benefit but also the benefits of all the others. Therefore, the driver's objective function can be formulated as

$$\begin{aligned} J_1(k) = \rho_1 E_1(k)^{\mathrm{T}} Q_1 E_1(k) + \rho_2 E_2(k)^{\mathrm{T}} Q_2 E_2(k) + \\ (1-\rho_1)\delta_1(k)^{\mathrm{T}}\delta_1(k) \end{aligned} \tag{48}$$

Equation (48) suggests that the driver not only accounts for their own path-tracking error $E_1(k)$ but also the AFS system's path-tracking error $E_2(k)$ when determining the driver's steering action $\delta_1(k)$.

In this context, Q_1 is the weighting matrix that regulates the relative importance assigned to the error in vehicle lateral displacement and that in its integral in $E_1(k)$.

$$Q_1 = \begin{bmatrix} q_1 & 0 & 0 \\ 0 & q_1 & 0 \\ 0 & 0 & q_1 \end{bmatrix}, \quad q_1 = \begin{bmatrix} q_1^y & 0 \\ 0 & q_1^{yint} \end{bmatrix} \tag{49}$$

where q_1^y and q_1^{yint} are the weighting factors associated with lateral displacement error and its integral, respectively.

Similarly, Q_2 is the weighting matrix for the AFS system's path-tracking $E_2(k)$ viewed by the driver.

$$Q_2 = \begin{bmatrix} q_2 & 0 & 0 \\ 0 & q_2 & 0 \\ 0 & 0 & q_2 \end{bmatrix}, \quad q_2 = \begin{bmatrix} q_2^y & 0 \\ 0 & q_2^{y_{int}} \end{bmatrix} \tag{50}$$

where q_2^y and $q_2^{y_{int}}$ are the weighting factors associated with lateral displacement error and its integral, respectively.

Note that Q_1 and Q_2 can take different values to reflect drivers' ability to place differing emphasis, from their own perspective, on penalizing the path-tracking errors of both themselves and the AFS controller.

In Eq. (48), ρ_1 and ρ_2 provide a global quantification of the relative emphasis assigned to the path-tracking errors of the driver and AFS. $\rho_1 + \rho_2 = 1$ always holds.

To facilitate the subsequent derivation, the driver's objective function Eq. (48) is rewritten as

$$J_1(k) = E(k)^{\mathrm{T}} Q E(k) + (1-\rho_1)\delta_1(k)^{\mathrm{T}}\delta_1(k) \tag{51}$$

where

$$\begin{gathered} E(k) = Z(k) - R(k), \\ R(k) = \begin{bmatrix} R_1(k) \\ R_2(k) \end{bmatrix}, \\ Q = \begin{bmatrix} \rho_1 Q_1 & 0 \\ 0 & \rho_2 Q_2 \end{bmatrix} \end{gathered} \tag{52}$$

Similarly, the AFS controller's objective function can be expressed as

$$J_2(k) = E(k)^{\mathrm{T}} Q E(k) + (1-\rho_2)\delta_2(k)^{\mathrm{T}}\delta_2(k) \tag{53}$$

The driver's steering strategy in the sense of Pareto equilibrium can be obtained by minimizing the cost function Eq. (51). This can be formulated as solving a least squares problem, as explained by Na and Cole [15]. The derivation begins by substituting Eq. (37) into Eq. (51), yielding

$$\begin{aligned} J_1(k) = {} & [\bar{\Theta}\delta_1(k) - \varepsilon_1(k)]^{\mathrm{T}} Q [\bar{\Theta}\delta_1(k) - \varepsilon_1(k)] + \\ & (1-\rho_1)\delta_1(k)^2 \end{aligned} \tag{54}$$

where $\varepsilon_1(k)$ is an intermediate term, taking the form of

$$\varepsilon_1(k) = R(k) - [\bar{\Psi} x(k) + \bar{\Omega}\delta_2(k)] \tag{55}$$

Equation (54) can be rewritten as

$$J_1(k) = \begin{bmatrix} S_Q[\bar{\Theta}\delta_1(k) - \varepsilon_1(k)] \\ S_{P1}\delta_1(k) \end{bmatrix}^{\mathrm{T}} \begin{bmatrix} S_Q[\bar{\Theta}\delta_1(k) - \varepsilon_1(k)] \\ S_{P1}\delta_1(k) \end{bmatrix} \tag{56}$$

where $S_Q{}^{\mathrm{T}} S_Q = Q$ and $S_{P1}{}^{\mathrm{T}} S_{P1} = 1 - \rho_1$.

Continuing to follow Ref. [15], the driver's steering angle $\delta_1(k)$ that minimizes Eq. (56) is the least-square solution of

$$\begin{bmatrix} S_Q\bar{\Theta} \\ S_{P1} \end{bmatrix} \delta_1(k) = \begin{bmatrix} S_Q \\ 0 \end{bmatrix} \varepsilon_1(k) \tag{57}$$

Then, $\delta_1(k)$ can be obtained by numerically solving Eq. (57) using the QR algorithm, yielding

$$\delta_1(k) = K_1 \varepsilon_1(k) \tag{58}$$

where

$$K_1 = \begin{bmatrix} S_Q\bar{\Theta} \\ S_{P1} \end{bmatrix} \backslash \begin{bmatrix} S_Q \\ 0 \end{bmatrix} \tag{59}$$

where symbol \ denotes the use of the QR algorithm for solving matrix equations in Matlab.

Substituting Eq. (55) into Eq. (58) to eliminate the intermediate term $\varepsilon_1(k)$

$$\delta_1{}^*(k) = G_1 \begin{bmatrix} x(k) \\ R(k) \end{bmatrix} + L_1\delta_2(k) \tag{60}$$

where $G_1 = [-K_1\bar{\Psi} \quad K_1]$ and $L_1 = -K_1\bar{\Omega}$. Equation (60) is the analytical expression of the driver's steering control strategy in the Pareto equilibrium sense. It can be seen that Eq. (60) is, in principle, consistent with the conceptual formulation of the driver's Pareto steering strategy presented in Eq. (44).

Following a similar procedure, the analytical expression of the AFS controller's Pareto steering strategy can be derived as

$$\delta_2{}^*(k) = G_2 \begin{bmatrix} x(k) \\ R(k) \end{bmatrix} + L_2\delta_1(k) \tag{61}$$

where G_2 and L_2 are matrices of appropriate dimensions. Equation (61) is, in principle, consistent with conceptual formulation of the AFS system's Pareto steering strategy given by Eq. (45).

It can be observed from Eqs. (60) and (61) that at time step k, $\delta_1{}^*(k)$, namely the driver's steering angle at the Pareto equilibrium explicitly depends on the AFS system's steering angle $\delta_2(k)$. Analogously, $\delta_2{}^*(k)$, the AFS system's steering angle at the Pareto equilibrium explicitly depends on the driver's steering angle $\delta_1(k)$. In practical engineering applications, such mutual dependency can be decoupled by modifying the driver's Pareto steering strategy Eq. (60) to

$$\delta_1{}^*(k) = G_1 \begin{bmatrix} x(k-1) \\ R(k) \end{bmatrix} + L_1\delta_2(k-1) \tag{62}$$

In the modified driver Pareto steering strategy given by Eq. (62), the driver's steering angle $\delta_1(k)$ at time step k now depends on the AFS controller's steering angle at the previous time step, denoted as $\delta_2(k-1)$ as well as the vehicle state $x(k-1)$. When the sampling interval of the discrete-time system is sufficiently small, the difference between $\delta_2(k)$ and $\delta_2(k-1)$, and that between $x(k)$ and $x(k-1)$ become negligible. As such, the modification introduced has little impact on the resulting value of $\delta_1(k)$. Equation (62) will thus serve as the basis for the identification of the driver's steering characteristics, as detailed later in this paper.

Once the modified driver Pareto steering strategy Eq. (62) is employed to determine the driver's steering angle at time step k, the AFS controller's Pareto steering strategy given by Eq. (61) can then be applied to compute the AFS controller's steering angle at the same time step k.

IV. Online Identification of Driver Steering Characteristics

In the driver's Pareto steering strategy given by Eq. (62), both matrices G_1 and L_1 are functions of A, B_1, B_2, C, N_1, q_2^y, $q_2^{y_{int}}$, q_1^y, and $q_1^{y_{int}}$. Here, A, B_1, B_2, and C are determined fully by the vehicle dynamics consideration q_2^y and $q_2^{y_{int}}$ are commonly specified as part of the AFS system's controller design. In contrast, q_1^y and $q_1^{y_{int}}$ are parameters characterizing the driver's steering behaviour, and generally exhibit variability across different drivers. Moreover, even for the same driver, these parameters may fluctuate because of changes in physical condition, mental state, or level of attention. As a result, q_1^y and $q_1^{y_{int}}$ are subject to temporal variation. Furthermore, q_1^y and $q_1^{y_{int}}$ affect the weighting matrix Q, which in turn influences the AFS system's determination of its steering angle according to Eq. (61). Therefore, it is necessary to identify q_1^y and $q_1^{y_{int}}$ online, to capture the driver's behaviour timely and adaptively.

From a technical standpoint, q_1^y and $q_1^{y_{int}}$ pose significant challenges. The difficulty arises from the fact that these two parameters are entangled with many other parameters, including A, B_1, B_2, C, N_1, q_2^y, and $q_2^{y_{int}}$ in the formulation of the driver's Pareto steering strategy Eq. (62). Consequently, the identification process may become overdetermined, potentially yielding multiple plausible solution sets. Given that the driver's steering characteristics are effectively determined by the combined influence of q_1^y and $q_1^{y_{int}}$ [27], we do not attempt to identify q_1^y and $q_1^{y_{int}}$ individually. Instead, it focuses on identifying the driver's steering control gain K_1, as defined by Eq. (59), which encapsulates the effects of both q_1^y and $q_1^{y_{int}}$.

A. Identification Approach

In this study, an online identification approach grounded on the recursive least squares method is developed to estimate the driver's steering control gain K_1. To ensure robust convergence and satisfactory identification performance under conditions of weak excitation, an exponential forgetting and resetting algorithm (EFRA) [29, 30] is incorporated. The core equations governing the proposed identification approach are written as

$$\hat{y}(k) = X(k)\hat{\Phi}^{\mathrm{T}}(k-1) \tag{63}$$

$$F(k) = \frac{\alpha P(k-1)X(k)}{\alpha + X^{\mathrm{T}}(k)P(k-1)X(k)} \tag{64}$$

$$\hat{\Phi}(k) = \hat{\Phi}(k-1) + F(k)\left[y(k) - \hat{y}(k)\right] \tag{65}$$

$$P(k) = \frac{1}{\lambda}\left[I - F(k)X^{\mathrm{T}}(k)\right] + \beta I - \gamma P^2(k-1) \tag{66}$$

where $\hat{y}(k)$ is the predicted output of the system model of interest at time step k, $\hat{\Phi}(k)$ is the parameter vector, taking the form of $\hat{\Phi}(k) = [\hat{\varphi}_1(k), \hat{\varphi}_2(k), ..., \hat{\varphi}_s(k)]$, $\hat{\varphi}_1(k)$, $\hat{\varphi}_2(k)$ up to $\hat{\varphi}_s(k)$ are the parameters to be estimated, $X(k)$ is the regression vector which is determined by the dynamics of the system model, $F(k)$ is the filter gain matrix, $P(k)$ is the covariance matrix, α is the filter coefficient, λ is the forgetting factor used to set different weights for the past and the new data, and β and γ are parameters used to adjust the covariance matrix respectively.

The procedure for implementing the identification approach described above can be summarized as follows:

(1) Initializing the covariance matrix through setting $P(0) = \sigma I$ with $\sigma \gg 0$, as well as the parameter vector through setting $\hat{\Phi}(0) = 0$.

(2) Computing the predicted model output $\hat{y}(1)$ using Eq. (63), and the filter gain matrix $F(1)$ using Eq. (64).

(3) Determining parameter vector $\hat{\Phi}(1)$ following Eq. (65) based on the $\hat{y}(1)$ and $F(1)$ obtained from the previous step, along with the measured model output $y(k)$.

(4) Determining the covariance matrix $P(2)$ according to Eq. (66), using the $F(1)$ obtained previously.

(5) Repeating steps (2) to (4) and continuing with the iteration.

B. Application of Identification Approach to Cooperative Game-Theoretic Driver-AFS Interaction

To apply the approach proposed above to identify driver steering characteristics within the framework of cooperative game-theoretic driver-AFS interaction, Eq. (62) is rewritten as

$$\delta_1{}^*(k) = \begin{bmatrix} -K_1(k)\bar{\Psi} & K_1(k) & -K_1(k)\bar{\Omega} \end{bmatrix} \begin{bmatrix} x(k-1) \\ R(k) \\ \delta_2(k-1) \end{bmatrix} \tag{67}$$

Equation (67) can be further rewritten as

$$\delta_1(k) = K_1(k)\chi(k) \tag{68}$$

where

$$\chi(k) = [-\bar{\Psi} \quad I \quad -\bar{\Omega}] \begin{bmatrix} x(k-1) \\ R(k) \\ \delta_2(k-1) \end{bmatrix} \tag{69}$$

In this study, it is acknowledged that a driver's steering characteristics may vary over time, even for the same individual, because of the changes in physical and mental states. Accordingly, the driver's steering control gain K_1 is not treated as a constant matrix. Instead, we focus on identifying a time-varying gain $K_1(k)$ at each discrete time step k, thereby capturing the dynamic nature of the driver's steering behaviour.

The following mapping can be established between the cooperative game-theoretic framework of the driver-AFS interaction, as illustrated in Fig. 1, and the theoretical basis of the online identification approach described by Eqs. (63)–(66).

$$\begin{aligned} &X(k) = \chi^{\mathrm{T}}(k), \\ &\hat{\Phi}(k) = K_1{}^{\mathrm{T}}(k), \\ &y(k) = \delta_1(k) \end{aligned} \tag{70}$$

In the context of the two-point preview setup introduced previously, $\chi(k)$ is a column vector of 18 × 1, as indicated in Eq. (69). Therefore, $K_1(k)$ is a row vector of 1 × 18. This dimensionality is computationally manageable for real-time identification purpose. In contrast, if the driver's or the AFS controller's path prediction, as discussed earlier, is set to span all 200 steps (corresponding to a preview time of 2 s and a discrete sampling interval of T = 0.01 s), the dimension of $K_1(k)$ will increase to 1 × 806. This highlights that the two-point preview setup, without compromising the fidelity in representing the driver's preview behaviour, can significantly reduce the computational burden, thereby enabling the online identification of driver steering characteristics.

On obtaining the driver's steering control gain $K_1(k)$, the weighting matrix $Q(k)$ can be subsequently determined.

This is carried out through the following procedure. First, Eq. (57) is left-multiplied by $\begin{bmatrix} \bar{\Theta}^{\mathrm{T}} S_Q{}^{\mathrm{T}} & S_{P1}{}^{\mathrm{T}} \end{bmatrix}$, resulting in

$$\delta_1(k) = \frac{\bar{\Theta}^{\mathrm{T}} Q(k)}{\bar{\Theta}^{\mathrm{T}} Q(k)\bar{\Theta} + 1 - \rho_1}\varepsilon_1(k) \tag{71}$$

Comparing Eq. (71) with Eq. (58) it can be seen that

$$K_1(k) = \frac{\bar{\Theta}^{\mathrm{T}} Q(k)}{\bar{\Theta}^{\mathrm{T}} Q(k)\bar{\Theta} + 1 - \rho_1} \tag{72}$$

It can be observed that the denominator on the right side of Eq. (72) is a non-zero scalar. Therefore, Eq. (72) can be rewritten as

$$M(k) = M(k)\bar{\Theta} K_1(k) + (1-\rho_1)K_1(k) \tag{73}$$

where

$$M(k) = \bar{\Theta}^{\mathrm{T}} Q(k) \tag{74}$$

Consequently, the weighting matrix $Q(k)$ can be determined by applying the QR algorithm to Eq. (74), such that

$$Q(k) = \bar{\Theta}^{\mathrm{T}} \backslash M(k) \tag{75}$$

where $M(k)$ can be computed numerically by rearranging Eq. (73) to the following form

$$M(k) = (1-\rho_1) K_1(k)[I - \bar{\Theta} K_1(k)]^{-1} \tag{76}$$

V. Numerical Study

Two numerical studies are conducted to examine the proposed cooperative game-theoretic framework for driver-AFS interaction. First, the driver's Pareto steering strategy, as defined in Eq. (62), is evaluated in a single-lane-change scenario. The objective is to assess whether the strategy, formulated based on the two-point-preview setup, can achieve satisfactory path-tracking performance. Second, effectiveness of the online identification approach introduced in this work is assessed in two cases that differ in the degree of similarity between the driver's and AFS system's target paths. These two numerical studies are detailed in the following two sections, respectively.

A. Numerical Study 1: Assessment of Vehicle Path-Tracking Performance under the Two-Point-Preview Steering Strategy

The vehicle parameters used in the simulation are provided in Table 1. The vehicle's longitudinal speed U is fixed at 20 m/s. The driver's preview time is set to 2 s. The sampling interval of the discrete-time system T is set to 0.01 s. In this numerical study, it is assumed that the AFS system is inactive, and the driver has full control of the vehicle. As a result, $\delta_2(k) = 0$, $\rho_1 = 1$, and $\rho_2 = 0$ hold. This assumption is considered reasonable, as the primary objective of the current numerical study is to assess whether the vehicle can deliver decent path-tracking performance under the two-point preview setup adopted in the driver's Pareto steering strategy. The driver's weighting factors for path-tracking errors, q_1^{y} and $q_1^{y_{int}}$ are both set to 0.1, i.e., $q_1^{y} = q_1^{y_{int}} = 0.1$. A single-lane-change scenario is employed.

Table 1 Vehicle parameter.

Symbol	Meaning	Value
m	Vehicle mass	1840 kg
C_{r}	Cornering stiffness of rear axles	187,000 N/rad
C_{f}	Cornering stiffness of front axles	116,000 N/rad
a	Distance from the vehicle's center of gravity to the front axles	1.136 m
b	Distance from the vehicle's center of gravity to the rear axles	1.663 m
I	Yaw moment of inertia	1430 kg·m^2
G	Steering gear ratio	15.8

The simulation results, including the profiles of vehicle paths and driver steering angles, are presented in Fig. 2. In Fig. 2(a), the red solid line denotes the driver's target path. The blue dashed line shows the vehicle path resulting from exercising the driver's Pareto steering strategy Eq. (62), based on the two-point preview setup. In contrast, the black solid line corresponds to the vehicle path obtained when the driver is assumed to adopt a "full preview", i.e., previewing all 200 steps within the 2 s preview window. It can be observed from Fig. 2(a) that both the two-point preview and the full preview setups exhibit satisfactory vehicle path-tracking performance. However, the two-point preview setup results in slightly larger overshoot in vehicle lateral deviation when entering the new lane, in comparison to the full preview setup.

Fig. 2(b) presents the profiles of the driver's steering angles obtained from the two-point preview and full preview setups: the blue dashed line shows the steering angle trajectory resulted from the two-point preview, while the blue solid line corresponds to that from the full preview. It can be observed that the steering angles generated by the two setups are closely aligned. Specifically, the peak steering angle associated with the two-point preview is slightly lower than that of the full preview. Moreover, the steering angle in the two-point preview setup returns to zero slightly later than in the full preview configuration. This observation is consistent with the difference in lateral deviation overshoot previously noted in Fig. 2(a).

Overall, the results from numerical study 1 demonstrate that

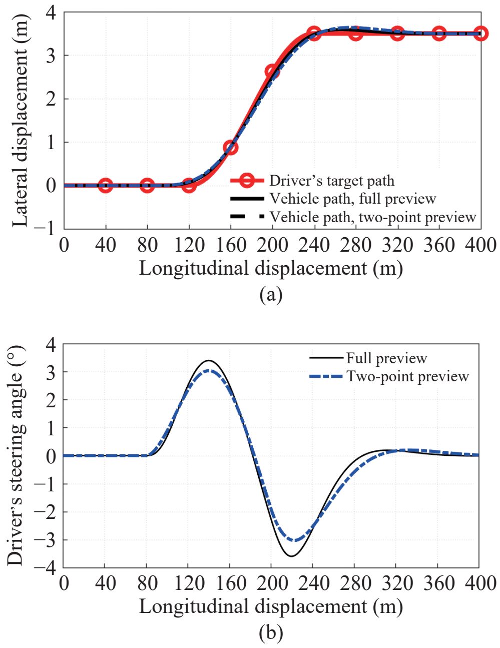

Fig. 2 Profiles of vehicle paths and driver steering angles, obtained in numerical study 1.

the driver's Pareto control strategy, when implemented using the two-point preview setup, achieves satisfactory vehicle path-tracking performance in the absence of AFS intervention. Notably, this performance is comparable to that achieved using the full preview setup, as evidenced by the closely aligned profiles of the driver's steering angles under both configurations.

B. Numerical Study 2: Assessment of Effectiveness of Online Identification of Driver Steering Characteristics

This section evaluates the effectiveness of the online identification approach introduced early in this paper. Note that the driver's Pareto steering strategy Eq. (62) considered in this study is based on the two-point preview setup.

To emulate realistic driving conditions, the driver's steering angle is superimposed by random noise prior to identification. The AFS system subsequently uses the identified driver characteristics to determine its steering angle through Eq. (61). Two cases are considered:

Case 1 The driver and active front steering system share the same target path.

Case 2 The driver and active front steering system hold different target paths.

While case 1 represents typical real-world conditions, case 2 allows investigation into the effects of differing weight distributions and parameter settings on vehicle path-following performance and driver steering angle profiles. The flow diagram of the numerical study is illustrated in Fig. 3, and the key parameters used in the identification approach are summarized in Table 2.

Fig. 4 illustrates the simulation results for case 1, where the driver imposes penalties on path-tracking errors using $q_1^y = 0.1$ and $q_1^{y_{int}} = 0$, and the AFS system using $q_2^y = 0.1$ and $q_2^{y_{int}} = 0$. ρ_1 and ρ_2, i.e., the parameters for allocating relative

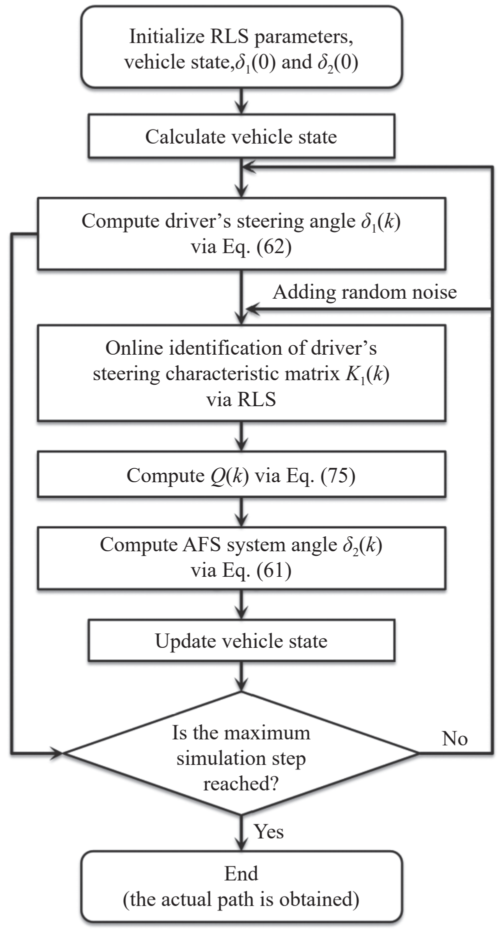

Fig. 3 Flow diagram of numerical study 2.

Table 2 Parameter in RLS algorithm.

Symbol	Parameter	Value
α	Filter gain	0.6
λ	Forgetting factor	0.98
β	Parameter for covariance resetting	0.006
γ	Parameter for covariance normalization	0.006
σ	Parameter for initializing the covariance matrix	0.5

weights for the driver's and AFS controllers' path-tracking activities are set as $\rho_1 = \rho_2 = 0.5$, indicating that the driver and AFS controller put equal emphasis on one another's path-tracking performance in their individual cost functions Eqs. (51) and (53).

In Fig. 4(a), the red solid line represents the driver's target path, the blue solid line represents the AFS system's target path, and black solid line denotes the vehicle trajectory. It can be observed that when both the driver and AFS share the same single-lane-change target path, the vehicle is able to accurately track the common target path.

Fig. 4(b) shows the steering angle profiles applied by the driver and AFS system. The red solid line denotes the driver's steering angle history, which is obtained by summing the output of the simulated Pareto steering strategy in Eq. (62), using the predefined driver weighting factors $q_1^y = 0.1$ and

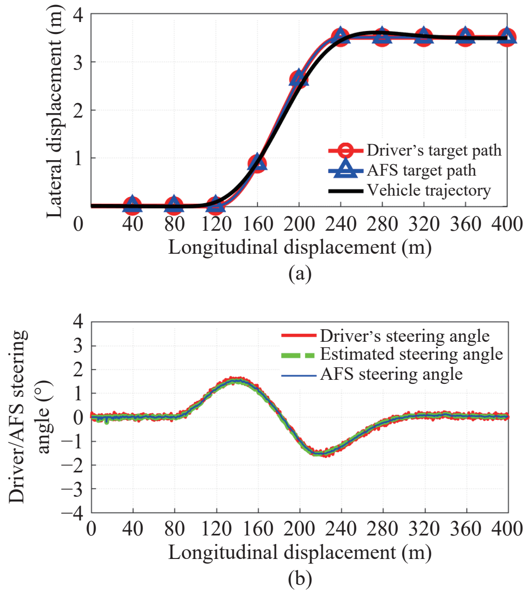

Fig. 4 Profiles of vehicle path, driver steering angle, and AFS steering angle, obtained in numerical study 2, case 1, under path-tracking weight allocation: $\rho_1 = \rho_2 = 0.5$; driver path-tracking penalties: $q_1^y = 0.1$ and $q_1^{yint} = 0$; and AFS path-tracking penalties: $q_2^y = 0.1$ and $q_2^{yint} = 0$.

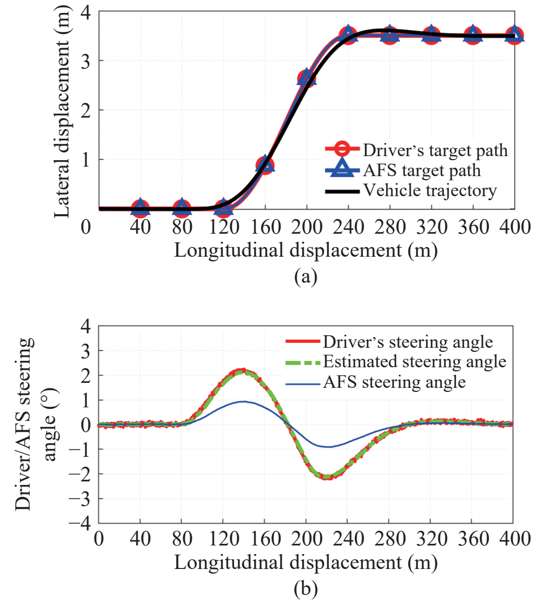

Fig. 5 Profiles of vehicle path, driver steering angle, and AFS steering angle, obtained in numerical study 2, case 1, under path-tracking weight allocation: $\rho_1 = 0.7$ and $\rho_2 = 0.3$; driver path-tracking penalties: $q_1^y = 0.1$ and $q_1^{yint} = 0$; and AFS path-tracking penalties: $q_2^y = 0.1$ and $q_2^{yint} = 0$.

$q_1^{yint} = 0$, and an added random noise component. As previously discussed, the inclusion of random noise is intentional and serves to emulate realistic measurements from vehicle sensors. The green dashed line that closely overlaps with the red line represents the estimated driver steering angle. This estimation is obtained using the weighting matrix $Q(k)$ identified via the online identification approach described in Section IV. The blue solid line denotes the AFS system's steering angle profile, determined using the identified $Q(k)$, along with the AFS controller's strategy Eq. (61).

It can be observed from Fig. 4 that the steering angle profiles of the driver and AFS are closely aligned, which is attributed to the equal weighting allocation $\rho_1 = \rho_2 = 0.5$. To further investigate the influence of weight allocation on vehicle path-tracking performance and the driver's and AFS controller's steering angle profiles, a different allocation $\rho_1 = 0.7$ and $\rho_2 = 0.3$ is adopted. This allocation implies that when optimizing the driver and AFS system cost function, greater emphasis is placed on minimizing the driver's path-tracking error, relative to that of the AFS. The corresponding numerical results are presented in Fig. 5.

As shown in Fig. 5(b), the steering angle profiles of the driver and AFS controller now exhibit noticeable differences. In particular, the amplitude of the driver's steering angle is significantly larger than that of the AFS system. In addition, the equal weight allocation $\rho_1 = \rho_2 = 0.5$ leads to driver's steering angle at about 1.5° during the lane change. However, when the driver's weight ρ_1 rises to 0.7, the driver's steering angle increases to around 2.1°, with a growth of 40%. These arises because, in addition to minimizing the deviation from their respective target paths, both the driver and AFS seek to minimize their own steering efforts, as defined in the driver and AFS system cost functions, Eqs. (51) and (53). Specifically, the driver's steering input is weighted by $1-\rho_1 = 0.3$, while the AFS controller's steering input is $1-\rho_2 = 0.7$. Since the driver's steering effort is penalized less heavily than that of the AFS, the resulting steering amplitude is correspondingly larger, as observed above.

Fig. 5(a) shows that the vehicle firmly follows the common target path of the driver and AFS. It can be seen that the vehicle path is identical to that shown in Fig. 4(a). This is because, when the driver and AFS controller share the same target path, minimizing either party's path-tracking error effectively serves the same objective—following the common target path. Consequently, the allocation of ρ_1 and ρ_2 has minimal influence on the resultant vehicle path. In addition, consistent with the findings presented in Fig. 4, the estimated driver steering angle shown in Fig. 5(b) (green dashed line) aligns closely with the driver steering angle with added noise (read solid line). This further validates the effectiveness of the online identification approach developed in this work.

Fig. 6 presents the results obtained using the same path-tracking weight allocation as in Fig. 5, i.e., $\rho_1 = 0.7$ and $\rho_2 = 0.3$, and the same path-tracking penalties applied by the AFS controller, i.e., $q_2^y = 0.1$ and $q_2^{yint} = 0$, but with different driver penalties: $q_1^y = 0.8$ and $q_1^{yint} = 1\times10^{-4}$. Fig. 6(a) further illustrates that the vehicle, jointly controlled by the driver and AFS system, tracks the target path firmly. Additionally, it can be seen that driver's penalties of $q_1^y = 0.8$ and $q_1^{yint} = 1\times10^{-4}$ lead to better path-tracking performance than that of $q_1^y = 0.1$ and $q_1^{yint} = 0$, despite a slightly large lateral.

As shown in Fig. 6(b), the proposed identification approach is capable of estimating the driver's steering characteristics accurately, yielding a reproduced steering angle profile (green dashed line) that closely matches the noise-perturbed driver steering input (read dashed line). However, Fig. 6(b) also depicts that the change of driver's penalties of $q_1^y = 0.8$ and

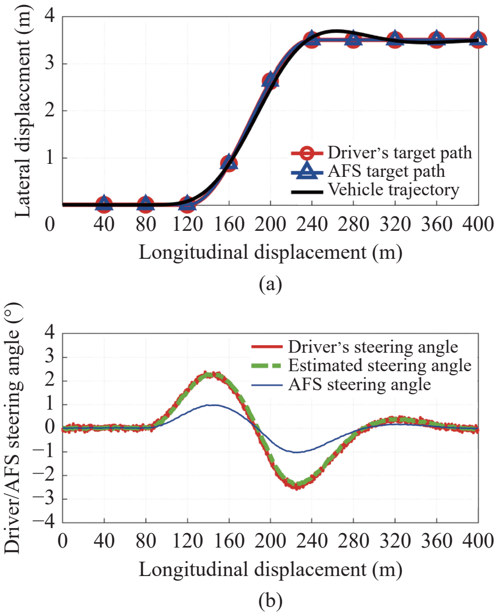

Fig. 6 Profiles of vehicle path, driver steering angle, and AFS steering angle, obtained in numerical study 2, case 1, under path-tracking weight allocation: $\rho_1 = 0.7$ and $\rho_2 = 0.3$; driver path-tracking penalties: $q_1^y = 0.8$ and $q_1^{yint} = 1\times10^{-4}$; AFS path-tracking penalties: $q_2^y = 0.1$ and $q_2^{yint} = 0$.

$q_1^{yint} = 1\times10^{-4}$ has negligible effects on the allocation of driver and AFS system steering angles.

Fig. 7 presents the numerical results for case 2, where the driver and AFS controller pursue different target paths. Specifically, as shown in Fig. 7(a), the driver aims to follow a straight-line target path (red solid line), whereas the AFS controller adheres to a single-lane-change target path identical in geometric profile to that used in case 1 (blue solid line). Here the driver imposes path-tracking penalties of $q_1^y = 0.1$ and $q_1^{yint} = 0$, while the AFS controller uses $q_2^y = 0.1$ and $q_2^{yint} = 0$. Regarding the path-tracking weight allocation between the driver and AFS controller, three distinct combinations of ρ_1 and ρ_2 are employed. Specifically, the vehicle path resulting from $\rho_1 = \rho_2 = 0.5$ is shown as black solid line, that from $\rho_1 = 0.8$ and $\rho_2 = 0.2$ as black dashed line, and that from $\rho_1 = 0.1$ and $\rho_2 = 0.9$ as black dash-dot line. For $\rho_1 = \rho_2 = 0.5$, the vehicle follows a path that lies approximately midway between the driver's and AFS controller's target paths. As ρ_1 increases to 0.8, the vehicle path shifts closer to the driver's straight-line target path. Conversely, when ρ_1 decreases to 0.1, the vehicle path approaches the active front steering controller's single-lane-change target path.

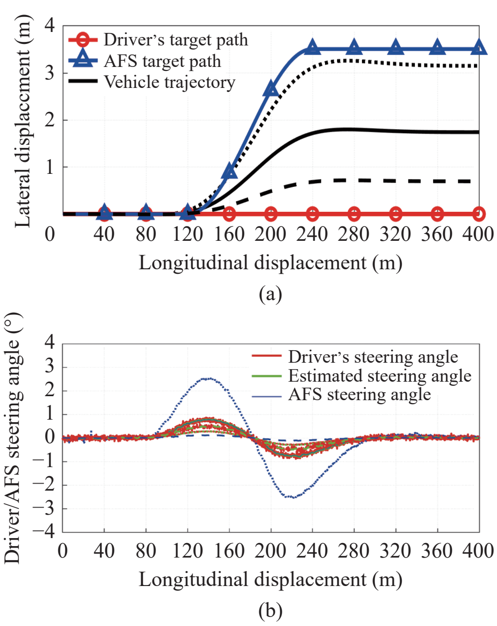

Fig. 7 Profiles of vehicle path, driver steering angle, and AFS steering angle, obtained in numerical study 2, case 2, under path-tracking weight allocations: $\rho_1 = \rho_2 = 0.5$ (solid line), $\rho_1 = 0.8$ and $\rho_2 = 0.2$ (dashed line), $\rho_1 = 0.1$ and $\rho_2 = 0.9$ (dotted line); driver path-tracking penalties: $q_1^y = 0.8$ and $q_1^{yint} = 0$; and AFS path-tracking penalties: $q_2^y = 0.1$ and $q_2^{yint} = 0$.

Fig. 7(b) illustrates the steering angle profiles of both the driver and AFS controller under different weight allocations. Specifically, results from the equal weight allocation, i.e., $\rho_1 = \rho_2 = 0.5$ are presented as solid lines, those from $\rho_1 = 0.8$ and $\rho_2 = 0.2$ as dashed lines, and those from $\rho_1 = 0.1$ and $\rho_2 = 0.9$ as dash-dot lines. First, it can be observed that the proposed online estimation approach accurately reproduces the driver's steering activities for all three cases. When equal weights are assigned, i.e., $\rho_1 = \rho_2 = 0.5$ (solid lines), the driver's and active front steering controller's steering angle profiles are identical.

When the driver is given a higher weight, i.e., $\rho_1 = 0.8$ and $\rho_2 = 0.2$ (dashed lines), both the driver's and AFS system's steering angles decrease, causing the vehicle to shift towards the driver's straight-line target path. However, the driver's steering exhibits a larger magnitude at about 0.5°, with a reduction of 50% compared with the steering angle resulted from equal weight allocation. Conversely, when the AFS controller is assigned a higher weight, i.e., $\rho_1 = 0.1$ and $\rho_2 = 0.9$ (dash-dot lines), its steering angle increases substantially, resulting in the vehicle shifting closer to the AFS controller's single-lane-change target path. Specially, the steering angle of AFS increases closely to 3° while the driver's steering angle drops to about 0.2°, compared with that both the driver's and AFS system's steering angles at about 1° under the equal weight allocation, i.e., $\rho_1 = \rho_2 = 0.5$.

Fig. 8 presents simulation results for the equal weight allocation, i.e., $\rho_1 = \rho_2 = 0.5$, but with three different combinations of the driver's and AFS controller's path-tracking error penalties: $q_1^y = q_2^y = 0.1$, as shown in solid lines; $q_1^y = 0.8$ and $q_2^y = 0.1$, as shown in dashed lines; and $q_1^y = 0.1$ and $q_2^y = 0.8$, as shown in dash-dot lines. Note that the penalties associated with the integral of the path-tracking errors are set as $q_1^{yint} = q_2^{yint} = 0$.

It can be observed in Fig. 8(a) that when the driver and AFS controller are assigned equal path-tracking error penalties, i.e., $q_1^y = q_2^y = 0.1$ (solid lines), the vehicle's path lies approximately midway between the driver's and AFS controller's target paths. However, when the driver uses a larger penalty, i.e., $q_1^y = 0.8$ and $q_2^y = 0.1$ (dashed lines), the vehicle's path shifts toward the driver's straight-line target

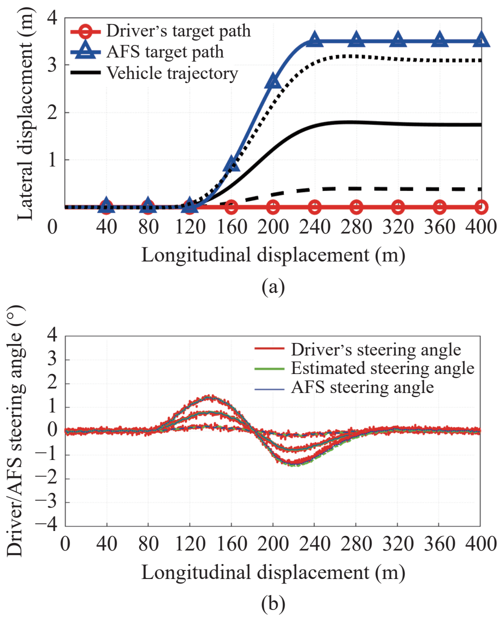

Fig. 8 Profiles of vehicle path, driver steering angle, and AFS steering angle, obtained in numerical study 2, case 2, under path-tracking weight allocation: $\rho_1 = \rho_2 = 0.5$; and driver and AFS path-tracking penalties: $q_1^y = q_2^y = 0.1$ (solid line), and $q_1^y = 0.8$ and $q_2^y = 0.1$ (dashed line) and $q_1^y = 0.1$ and $q_2^y = 0.8$ (dotted line).

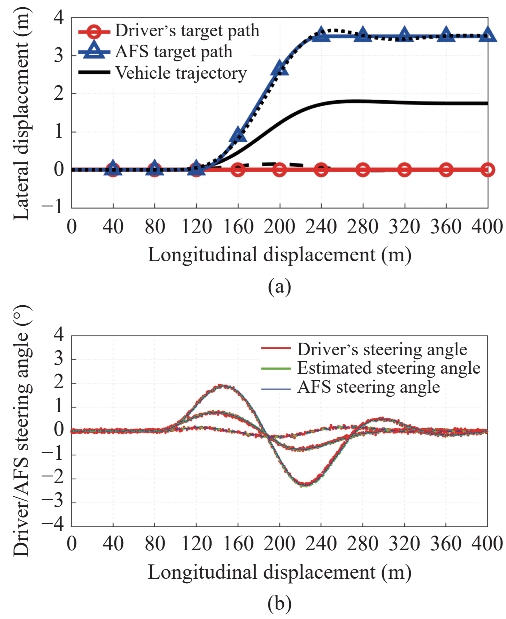

Fig. 9 Profiles of vehicle path, driver steering angle, and AFS steering angle, obtained in numerical study 2, case 2, under path-tracking weight allocation: $\rho_1 = \rho_2 = 0.5$; and driver and AFS path-tracking penalties: $q_1^{yint} = q_2^{yint} = 0$ (solid line), $q_1^{yint} = 1\times10^{-4}$ and $q_2^{yint} = 0$ (dashed line) and $q_1^{yint} = 0$ and $q_2^{yint} = 5\times10^{-4}$ (dotted line).

path. Conversely, when the AFS controller employs a larger penalty, i.e., $q_1^y = 0.1$ and $q_2^y = 0.8$ (dash-dot lines), the vehicle's path shifts towards the AFS controller's single-lane-change target path.

It can be observed in Fig. 8(b) that the proposed identification approach gives accurate estimation of driver steering activities again. Moreover, the driver's and AFS controller's steering angle profiles are always identical, because of the equal weight allocation, as analyzed previously. In addition, the driver's (and the AFS controller's) steering angles increase as the AFS controller's weight increases, because the AFS controller's single-lane change target path requires larger steering efforts.

The previous section analyzed the effects of path-tracking penalties q_1^y and q_2^y on the vehicle's actual trajectory and steering inputs. From Figs. 7 and 8, it can be observed that a steady-state tracking error exists between the actual vehicle trajectory and the target path. This is because parameters associated with the integral of path tracking errors, q_i^{yint}, $i = 1,2$, are set to zero or a value that is too small to be neglected. Next, the effects of these parameters on the actual vehicle trajectory will be further analyzed.

Fig. 9 presents simulation results illustrating the effects of different parameters q_1^{yint} and q_2^{yint}. In particular, three different combinations of q_1^{yint} and q_2^{yint} are considered in this simulation: (1) $q_1^{yint} = q_2^{yint} = 0$, as shown in solid lines, (2) $q_1^{yint} = 1\times10^{-4}$ and $q_2^{yint} = 0$, as shown in dashed lines, and (3) $q_1^{yint} = 0$ and $q_2^{yint} = 5\times10^{-4}$, as shown in dotted lines. In addition, both penalties q_1^y and q_2^y are set as 0.1 and the equal weight allocation is set, i.e., $\rho_1 = \rho_2 = 0.5$.

As shown in Fig. 9(a), when $q_1^{yint} = q_2^{yint} = 0$, the actual vehicle trajectory lies approximately midway between the driver's and AFS system's target paths. When the driver's parameter q_1^{yint} is increased ($q_1^{yint} = 1\times10^{-4}$ and $q_2^{yint} = 0$), the vehicle's actual trajectory becomes clearly biased toward the driver's target path. Additionally, the vehicle can better track the driver's path accurately, without steady-state tracking errors. Comparatively, when the parameter q_2^{yint} is increased ($q_1^{yint} = 0$ and $q_2^{yint} = 5\times10^{-4}$), the vehicle shifts towards the AFS system's target path, resulted from larger steering angles (about 2°) of both the driver and AFS than that under the case of $q_1^{yint} = q_2^{yint} = 0$. Moreover, the vehicle can follow the AFS system's target path, again without steady-state tracking errors. Fig. 9(b) indicates steering angles of the driver and AFS under different q_1^{yint} and q_2^{yint} settings. The underlying variation mechanism is similar to that for q_1^y and q_2^y and will not be repeated here.

VI. Conclusion

This work addresses the challenges of understanding and modelling the influence of vehicle automation on driver steering behaviours, and accommodating variability of steering characteristics amongst drivers. A cooperative game-theoretic framework for driver-automation interaction control is developed, incorporating an online identification approach to estimate driver steering characteristics.

Numerical results demonstrate that the proposed Pareto-equilibrium steering strategy, incorporating a two-point preview setup achieves desirable vehicle path-tracking performance. Moreover, the results indicate that variations in the driver's and AFS controller's control authority weights and their path-tracking penalties can significantly influence the vehicle's actual path and the two control authorities' steering angle profiles. Finally, the effectiveness of the proposed online identification approach is validated under various combinations of the control authority weights and driver and AFS path-tracking penalties.

In future, the identification approach will be examined using real-world experiments involving human drivers, using a driving simulator and/or an instrumented test vehicle.

Acknowledgment

This study was supported by the National Key R&D Program of China (No. 2023YFB4302600), the "Pioneer" and "Leading Goose" R&D Program of Zhejiang (No. 2023C03155), the State Key Laboratory of Biobased Transportation Fuel Technology, the ZJU-YST Joint Research Center for Fundamental Science, the Smart Urban Future (SURF) Laboratory, Zhejiang Province, the Sustainable Smart Liveable Cities Research Centre, Zhejiang Province, the Zhejiang University Global Partnership Fund, and the Zhejiang University Sustainable Smart Livable Cities Alliance (SSLCA).

References

[1] J. Qi, Study on driving fatigue based on ergonomics, *Adv. Mater. Res.*, 2013, 706–708, 2119–2123.

[2] S. Zhu, Y. Li, and T. Liu, Factors affecting the driver in traffic accidents, *Automob. Appl. Technol.*, 2015, 12(4), 144–145, (in Chinese).

[3] Y.-F. Hu, T. Qu, J. Liu, Z.-Q. Shi, B. Zhu, D.-P. Cao, and H. Chen, Human-machine cooperative control of intelligent vehicle: Recent developments and future perspectives, *Acta Autom. Sin.*, 2019, 45(7), 1261–1280, (in Chinese).

[4] S. Payandeh, A brief overview study of open quantum system for application in human-machine interaction, *Int. J. Intell. Control Syst.*, 2024, 29(4), 164–170.

[5] W. Scholtens, S. Barendswaard, D. Pool, R. Van Paassen, and D. Abbink, A new haptic shared controller reducing steering conflicts, in *Proc. 2018 IEEE International Conference on Systems, Man, and Cybernetics (SMC)*, Miyazaki, Japan, 2018, 2705–2710.

[6] H. M. Zwaan, S. M. Petermeijer, and D. A. Abbink, Haptic shared steering control with an adaptive level of authority based on time-to-line crossing, *IFAC-PapersOnLine*, 2019, 52(19), 49–54.

[7] A. T. Nguyen, C. Sentouh, and J. C. Popieul, Driver-automation cooperative approach for shared steering control under multiple system constraints: Design and experiments, *IEEE Trans. Ind. Electron.*, 2017, 64(5), 3819–3830.

[8] M. R. Oudainia, C. Sentouh, A. T. Nguyen, and J. C. Popieul, Dynamic conflict mitigation for cooperative driving control of intelligent vehicles, in *Proc. 2022 IEEE Intelligent Vehicles Symposium (IV)*, Aachen, Germany, 2022, 1445–1452.

[9] H. Chen, Y.-Y. Guo, J. Liu, H.-Y. Guo, and M.-Y. Cui, Design of human-vehicle torque collaborative steering controller based on driving state prediction, *Control Decis.*, 2019, 34(11), 2390–2396, (in Chinese).

[10] J. Han, J. Zhao, and B. Zhu, Variable impedance-based human-machine interaction method using reinforcement learning for shared steering control of intelligent vehicle, *J. Mech. Eng.*, 2022, 58(18), 141–149, (in Chinese).

[11] F. Ding, Q. Li, F. Lei, and J. Liu, Research on human-machine shared steering predictive control strategy assisted with torque correlation under dynamic trajectory tracking, *J. Mech. Eng.*, 2022, 58(6), 143–152, (in Chinese).

[12] Y. Lu, J. Liang, G. Yin, L. Xu, J. Wu, J. Feng, and F. Wang, A shared control design for steering assistance system considering driver behaviors, *IEEE Trans. Intell. Veh.*, 2023, 8(1), 900–911.

[13] X. Na and D. J. Cole, Game-theoretic modeling of the steering interaction between a human driver and a vehicle collision avoidance controller, *IEEE Trans. Hum. Mach. Syst.*, 2015, 45(1), 25–38.

[14] X. Na and D. J. Cole, Modelling of a human driver's interaction with vehicle automated steering using cooperative game theory, *IEEE/CAA J. Autom. Sin.*, 2019, 6(5), 1095–1107.

[15] X. Na and D. J. Cole, Experimental evaluation of a game-theoretic human driver steering control model, *IEEE Trans. Cybern.*, 2023, 53(8), 4791–4804.

[16] X. Ji, K. Yang, X. Na, C. Lv, and Y. Liu, Shared steering torque control for lane change assistance: A stochastic game-theoretic approach, *IEEE Trans. Ind. Electron.*, 2019, 66(4), 3093–3105.

[17] M. Li, X. Song, H. Cao, J. Wang, Y. Huang, C. Hu, and H. Wang, Shared control with a novel dynamic authority allocation strategy based on game theory and driving safety field, *Mech. Syst. Signal Process.*, 2019, 124, 199–216.

[18] K. Yang, Y. Liu, X. Na, X. He, Y. Liu, J. Wu, S. Nakano, and X. Ji, Preview-scheduled steering assistance control for co-piloting vehicle: A human-like methodology, *Veh. Syst. Dyn.*, 2020, 58(4), 518–544.

[19] J. Liu, W.-Q. Shi, H.-Y. Guo, Q.-K. Dai, and Z.-H. Gao, Stackelberg game based driver-automation cooperative steering control with dynamic driving authority, *China J. Highw. Transp.*, 2022, 35(3), 127–138, (in Chinese).

[20] J. Liang, Y. Lu, F. Wang, J. Feng, D. Pi, G. Yin, and Y. Li, ETS-based human–machine robust shared control design considering the network delays, *IEEE Trans. Autom. Sci. Eng.*, 2025, 22, 17501–17511.

[21] S. Jiao, Q. Wei, F. Dai, J. Wu, M. Qiu, B. Zhang, Y. Luo, K. Huang, and G. Ma, Event-based cooperative control for uncertain multiagent system using parallel adaptive dynamic programming, *Int. J. Intell. Control Syst.*, 2024, 29(3), 127–133.

[22] J. Lu, Q. Wei, and X. Cheng, Event-based optimal control for cooperative adaptive cruise control, *Int. J. Intell. Control Syst.*, 2025, 30(2), 176–181.

[23] Z. Fang, J. Wang, Z. Wang, J. Liang, Y. Liu, and G. Yin, A human-machine shared control framework considering time-varying driver characteristics, *IEEE Trans. Intell. Veh.*, 2023, 8(7), 3826–3838.

[24] D. J. Cole, Occupant-vehicle dynamics and the role of the internal model, *Veh. Syst. Dyn.*, 2018, 56(5), 661–688.

[25] A. Y. Ungoren and H. Peng, An adaptive lateral preview driver model, *Veh. Syst. Dyn.*, 2005, 43(4), 245–259.

[26] S. D. Keen and D. J. Cole, Bias-free identification of a linear model-predictive steering controller from measured driver steering behavior, *IEEE Trans. Syst. Man Cybern. Part B Cybern.*, 2012, 42(2), 434–443.

[27] X. Na, Game theoretic modelling of a driver's steering interaction with active steering, PhD dissertation, University of Cambridge, UK, 2014.

[28] Y. Xing, C. Lv, H. Wang, D. Cao, E. Velenis, and F.-Y. Wang, Driver activity recognition for intelligent vehicles: A deep learning approach, *IEEE Trans. Veh. Technol.*, 2019, 68(6), 5379–5390.

[29] M. E. Salgado, G. C. Goodwin, and R. H. Middleton, Modified least squares algorithm incorporating exponential resetting and forgetting, *Int. J. Control*, 1988, 47(2), 477–491.

[30] Z. Ercan, A. Carvalho, M. Gokasan, and F. Borrelli, Modeling, identification, and predictive control of a driver steering assistance system, *IEEE Trans. Hum. Mach. Syst.*, 2017, 47(5), 700–710.

Yue Liu received the PhD degree in automotive engineering from Beihang University, China, in 2023. She is currently a postdoctoral researcher at Zhejiang University, China. Her research interests include driver-vehicle dynamics, control theory, driver-automation shared control, and sustainable development of road freight.

Simon Hu received the PhD degree from Imperial College, London, UK, in 2011. He is currently an associate professor at Zhejiang University-University of Illinois at Urbana-Champaign Institute, Zhejiang University, Haining, China, and an honorary research fellow at Imperial College, London, UK. His research interests include intelligent transportation systems, connected and automated vehicles, smart mobility, and transportation electrification.